Numerical simulation of transversely impacted, clamped circular aluminium plates

Richard Villavicencio, Leight Sutherland and Carlos Guedes Soares

Centre for Marine Technology and Engineering (CENTEC), Technical University of Lisbon, Instituto Superior Técnico, Lisboa, Portugal.

Abstract:
In this paper experimental and numerical results of a series of drop weight impact tests examining the dynamic response of fully clamped aluminium 5083/H111 circular plates struck transversely at the centre by a mass with a spherical indenter are presented. The impact velocity varied from 1.0 to 6.0 m/s. The plates showed no visible damage at the very lowest incident energies, but suffered both indentation damage and plastic deformation as incident energy was increased. The numerical modelling was performed using the LS-DYNA non-linear, dynamic finite element software. Both shell and solid element models of progressively refined mesh sizes were used and the results compared with the experimental data. The numerical calculations used can accurately predict the response of deflections, forces and absorbed energies, even for the models with coarse meshes. However, finer meshes and solid elements were required to obtain a satisfactorily accurate prediction of the deformed shape.

Introduction

Increased attention is being paid to the assessment of the collision strength of ship structures, and to developing more crashworthy designs. One approach to the problem is to use complex finite element models to calculate the energy absorbed during collision (Akita et al. 1972, Kajaste-Rudnitski et al. 2005). Another approach is to use simple models of energy absorption for each structural member and to calculate the absorbed energy as the collision progresses and the structural elements are subjected to large deformations (McDermott et al. 1974, Amdhal et al. 1995, Wang et al. 1997). The simplified models used to calculate energy absorption are based on rigid plastic theory, which has been shown to be appropriate for these predictions as described in Guedes Soares (1981), Jones (1989), Stronge and Yu (1993), and Yu and Chen (2000), among others. Concerning the behaviour of plates, a theoretical analysis that examines the dynamic plastic response of thin circular plates transversely and centrally struck by a mass with a conical head and a spherical nose has been summarized by Shen (1995). The analysis employs an interaction yield surface which combines the bending moment and membrane forces required for plastic flow. Approximate formulas for the load-deflection relationship of a rigid-plastic circular plate deflected by a rigid sphere were derived by Wang et al. (1998), which studied the behaviour at large deflection, neglecting the contribution from bending moments. Mechanics of the lateral indentation of a rigid sphere into a thin, ductile metal plate were studied by Simonsen and Lauridsen (2000) including experiments, analytical theories and finite elements calculations. The focus was the prediction of plate failure and the energy absorption until this point. Analytical theories were derived for the load-displacement behaviour of a plastic membrane up to failure. Experimental tests which examine the dynamic response and petalling failure of thin circular plates struck transversely by masses having conical heads were conducted by Shen et al. (2002) and the theoretical analysis which examines the petalling failure was proposed by Shen (2002).

The purpose of the present work is to compare the results of a series of experimental tests previously reported by Sutherland and Guedes Soares (2009) with a finite element analysis using different elements type and meshes size. The force-displacement curves of the different simulations are compared with the experimental results and the best approximations are selected for further calculations. The shape of the deformation is analyzed considering local indentation and global deflections.

Theoretical background

A theoretical analysis of the dynamic plastic response of thin circular plates struck transversely by non-blunt masses was proposed by Shen (1995) and is summarized as follows; The fully clamped circular plate in Figure 1 has a radius R, thickness H, mass density ρ and is struck by a mass G traveling with an initial velocity V_0 at the centre of the plate. After impact, the striker G is assumed to remain in contact with the plate. Therefore, the striker and the struck point of the plate have an initial velocity V_0 at the instant of contact and a common velocity throughout the entire response. The maximum total deformation W_t is divided into two parts: maximum local indentation W_i and maximum global deflection W. A quasi-static method is used to analyze the local deformation, while the global deflection is studied with a dynamic analysis. The local indentation and the central global deflection correspond to a common force magnitude between the striker and the impact point of the plate throughout the whole response. First the global deflection is calculated along with its corresponding force, and from this force the indentation is calculated. Thus, for example, the maximum force corresponds to the maximum centralglobal deflection and the maximum local indentation.

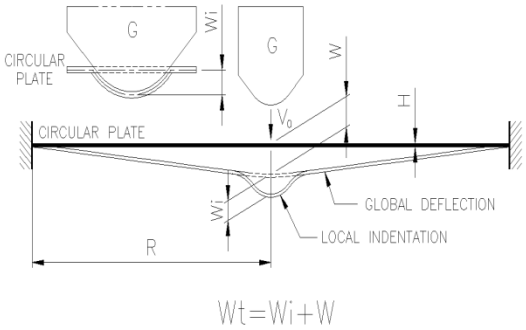

Figure 1: Clamped circular plate struck transversely at the centre by a mass.

The yield condition combines the bending moment and membrane force which cause the cross-section of a perfectly plastic structure to became fully plastic (Jones 1989). Material strain rate sensitive effects are considered with the aid of the Cowper-Simonds equation and Perrone and Bhadras approximation, which was further simplified by Jones (1989).

The indentation of the plate under the striker is observed to have the same shape as the head of the striker. It is assumed that any point in the un-deformed plate moves vertically without horizontal displacement in the deformed plate, as can be seen in the detail of Figure 1. For the global deflection the following two simplifications are introduced:

(a) The radial and circumferential membrane forces are equal and are independent of the radial coordinate.
(b) Plastic yielding is controlled independently by radial and circumferential bending moments and membrane forces.

In view of assumption (a) the normality requirement of plasticity associated with circumferential bending moment and membrane force is disregarded. Figure 1 shows the permanent total deformation of the plate, the shape of the un-deformed plate and the global deformation of the plate without local indentation. The local indentation plays an important role in the total response of the plate (W_i *and* W are generally of similar magnitude) and hence cannot be neglected.

Experimental details and summary of results

Impact testing was performed using a fully instrumented Rosand IFW5 falling weight machine. A small, light hemispherical ended cylindrical projectile was dropped from a known, variable height between guide rails onto clamped horizontally supported circular aluminium 5083/H111 plate targets. A much larger, variable mass was attached to the projectile and a load cell between the two gave the variation of impact force with time. An optical gate gave the incident velocity of the impact head, and hence the velocity, displacement and the energy it imparted could be calculated from the measured force-time data by successive numerical integrations, knowing the impact mass. The experimental set up can be seen in Figure 2. Specimen plates were 200 mm square and were fully clamped by four bolts between two thick 200 mm square steel plates with internal diameter D = 100 mm. The indenter was a hemi-spherically ended projectile of radius r = 5 mm. In order to investigate the effects of both global deformation and local indentation, tests were carried out for two plate thickness', 2.0 mm and 5.92 mm, (henceforth referred to as 'thin' and 'thick' respectively) using an impact mass of 3.103 kg and 4.853 kg respectively. Tests were carried out on virgin specimens for a range of impact velocities, from very low energies up to perforation where possible. Full experimental details and discussions of the experimental results may be found in Sutherland and Guedes Soares (2009).

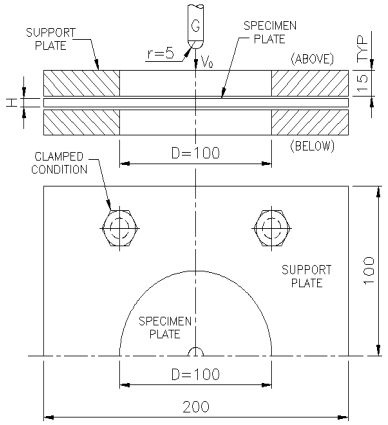

Figure 2: Circular plate specimen in clamped condition (dimensions in millimetres).

A representative sample of the full experimental results at low, medium and high incident energy for both thin and thick plates were selected for comparisons with the current numerical analyses, and are summarised in Table 1. The 'End' of the test is defined as when the contact force drops to zero, and occurs when the indenter first leaves the surface of the plate. Specimens suffering perforation were not considered here.

Table 1: Summary of experimental impact results.

Specimen	Impact Velocity (m/s)	Values at Peak Force			Values at End	
		Force (kN)	Defln (mm)	Energy (J)	Defln (mm)	Energy (J)
AL1-K	0.95	1.2	2.50	1.6	1.27	1.1
AL1-N	2.53	3.7	5.36	10.6	4.07	9.1
AL1-R	4.39	6.7	9.99	31.2	8.98	29.8
AL1-U	5.90	8.9	12.78	55.7	12.00	55.1
AL2-H	0.91	4.8	0.79	2.3	0.23	1.1
AL2-I	2.62	11.4	2.41	16.8	1.23	12.2
AL2-B	4.77	15.8	5.30	56.8	4.19	52.2
AL2-D	5.85	18.4	6.74	84.0	5.79	80.2

Numerical model

The computations were carried out using the LS-DYNA (version 971, Hallquist 2005) finite element package which is appropriate for non-linear explicit dynamic simulations with large deformations. The finite element model was designed with the following components (Figures 3 and 4): specimen plate, two support plates (one below and the other above the specimen plate) and the striking mass. The specimen

plates were modelled with either shell or solid elements, the support plates with shell elements, and the striking mass with solid elements. The shell elements were 4-node with 5-integration points thought the thickness (Belytshko-Tsay formulation) and the solid elements were 8-node with 1-integration point (constant stress solid element formulation), both element formulations are the default in LS-DYNA.

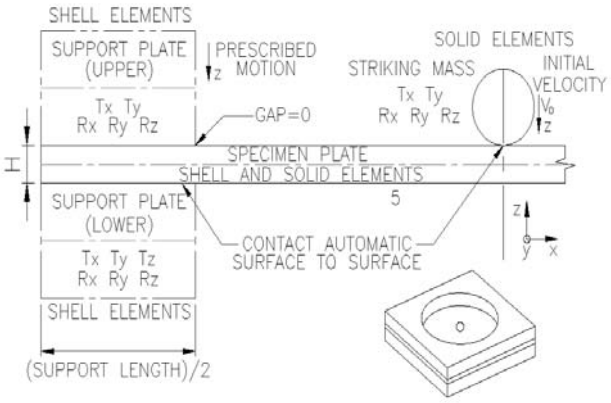

Figure 3: Details of finite element model.

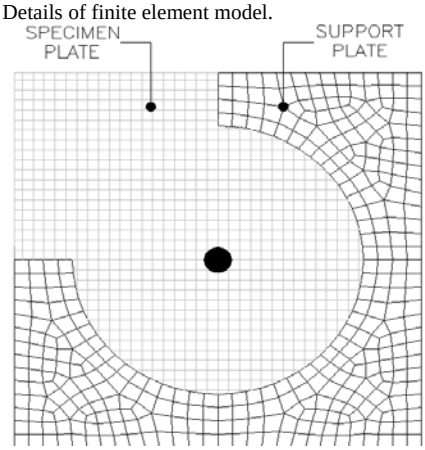

Figure 4: Typical mesh.

Mesh design

The type of element (shell or solid) and the mesh size used to model the plates were varied in order to optimise the agreement of the FE model with the experimental results. The meshing used in all cases was regular and square (Figure 4), meaning that the mesh was not finer neither at the point of impact nor at the supported perimeter. Initial calculations explored the use of different mesh configurations, some of them automatically generated and others with coincident nodes in the supports and radial orientation of the elements. Similar results were obtained in all cases and hence the simplest and cheapest mesh design was selected for all future calculations.The approach taken was to start with a mesh size equal to the plate thickness and then progressively decrease the mesh size until good correlation with the experimental maximum force and displacement results was achieved. It was also important to obtain a good approximation of the shape of the plate deformation, in terms of both local indentation and global deflection. The mesh size of the shell element models considered were 6x6, 4x4 and 2x2 mm for the thick plates (denoted by Shell6, Shell4 and Shell2 respectively), and 2x2, 1x1 and 0.5x0.5 mm for the thin plates (denoted by Shell2, Shell1 and Shell0.5 respectively). Care was taken to avoid an excessively high element side length to thickness ratio. The solid element model mesh sizes were 1x1x1mm for the thin plates (Solid1), and 2x2x2 and 1x1x1 mm for the thick plates (Solid2 and Solid1 respectively).

The finite element representation of the support plates was used to simulate the experimentally clamped boundary condition of the specimen plates using a relatively coarse mesh of shell elements with a side length of approximately 5 mm. The striking mass was modelled using solid elements since this simplified the definition of both the impact mass and the geometry, and in order to model the spherical geometry sufficiently accurately a mesh size of approximately 1.0 mm was chosen. The sphere was meshed to ensure that the face of a sphere element (as apposed to a single node 'corner') contacted with the plate, ensuring a more realistic simulation of the contact area.

The radius of the impacting mass is 5.0 mm, and hence the ratios of element size to indenter radius were 6/5, 4/5, 2/5, 1/5 and 1/10 for meshes with element side length 6, 5, 4, 2, 1 and 0.5 mm respectively. These ratios play an important role when the shape of the deformation is analyzed.

Boundary conditions

In the present finite element model the support plates simulate the boundary conditions of the specimen plate, compressing the specimen as occurred in the experiments (Figure 3). Only half of the support plate length compressing the specimen was modelled since this reduced the computational cost whilst previous numerical analyses showed that this did not affect the results. However, differences in the maximum displacement and absorbed energy were seen when the support plate thickness was reduced, and hence the full support plate thickness was modelled. No gap between the support plates and the specimen plate was modelled.

The lower support plate was constrained in all degrees of freedom (Figure 3). The upper support plate was constrained in all degrees of freedom except for vertical translation, because a prescribed vertical motion was imposed to compress the specimen plate to simulate the clamped condition. The value of the prescribed displacement was equal to $\varepsilon_y H/3$ (Ehlers 2010), where ε_y is the yield strain of the material and H is the thickness of the specimen. For the striking mass only the vertical translation was free, in which direction the initial impact velocity V_0 was assigned.

Contact definition

The contact between the striking mass and the specimen plate and between the support plates and the specimen plate were defined as "Automatic Surface to Surface" (Hallquist 2005). A static coefficient of friction of 0.3 in both cases was used and a dynamic coefficient of friction of 0.1 was included in the contact

between the striking mass and specimen plate (Ehlers et al. 2007, Ehlers 2010).

Material

Both support plates were modelled as a rigid material to ensure no deformation. The 'Mat.020-Rigid' was selected from the material library of LS-DYNA, assigning mild steel mechanical properties (Young's modulus 210 GPa and Poisson's ratio 0.3) and a mass density of 7850 kg.

The striking mass was modelled using the same rigid un-deformable material and mechanical properties as the support plates. However, since the falling weight assembly was modelled as a simple sphere, an artificially large density was used to give the same mass as used in the experiments. The mass densities were 6.5E+6 and 10.0E+6 kg/m^3 for the striking mass of 3.103 and 4.853 kg respectively (a factor of 1.035 was included to allow for the small volume error since the sphere was modelled with a finite number of discrete flat elements).

The definition of the specimen plate material is most important, and thus the mechanical properties of the material used in the finite element models were obtained from in-house tensile tests carried out on material cut from the same panels from which the impact specimens were taken, and are summarized in Table 2. The material selected from the library of LS-DYNA was 'Mat.024-Piecewice linear plasticity', which allows the definition of a true stress-strain curve as an offset table.

Table 2: Mechanical properties of aluminium 5083/H111.

Property	Units	Aluminium 2.0 mm	Aluminium 6.0 mm
Mass density	kg/m^3	2710	2710
Young's modulus	GPa	65	65
Poisson's ratio	-	0.33	0.33
Yield stress	MPa	125	145
Rupture stress	MPa	285	290

Since the engineering stress-strain curve does not give a true indication of the deformation characteristics of a metal, it is necessary to use the true stress-strain curve that represents the basic plastic-flow characteristics of the material. The true stress must be based on the actual cross-sectional area of the specimen, but the true strain measurement is measured directly when, as is the case here, strain gauges are used (Dieter 1986).

In the true stress-strain curve until the onset of necking (for most materials, necking begins at maximum load at a value of strain where the true stress equals the slope of the flow curve) the true stress σ_t and the true strain ε_t are expressed in terms of engineering stress σ_e and engineering strain ε_e by:

$$\sigma_t = \sigma_e(\varepsilon_e + 1) \quad (1)$$

$$\varepsilon_t = \ln(\varepsilon_e + 1) \quad (2)$$

The tensile tests of these particular aluminum plates showed that the true stress at maximum load is almost coincident with the true fracture stress, and also noting that very little necking was observed in the tensile tests, the exact true stress-strain curve can be used as input in the numerical models. The true and engineering stress-strain curves for each thickness are shown in Figures 5 and 6. Since for the experimental impact tests considered here only plastic deformation was observed, failure strain was not required to define the material of the specimen plates.

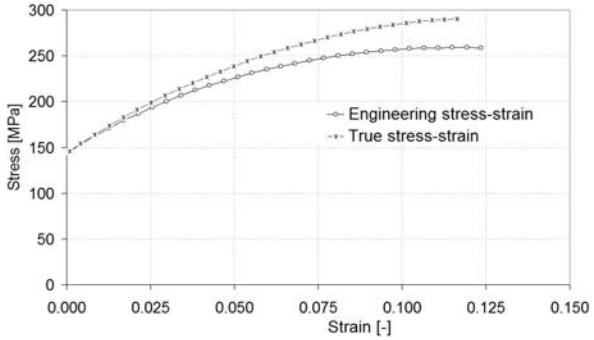

Figure 5: Engineering and true stress-stain curves (experimental). Thickness 5.92 mm.

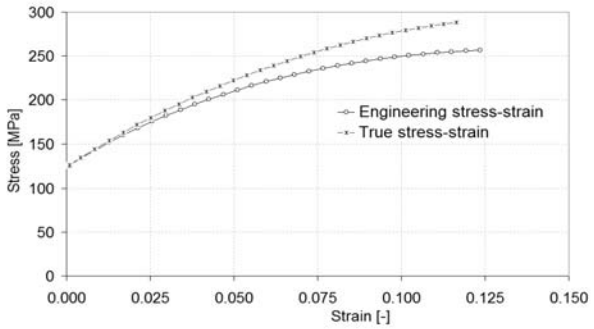

Figure 6: Engineering and true stress-stain curves (experimental). Thickness 2.00 mm.

The strain-rate sensitivity behaviour of materials in the finite element model may be included using the coefficients of the Cowper-Simonds constitutive equation (Jones 1989). However, published experimental results for aluminium alloy beams (Liu and Jones 1987) showed that they are essentially strain-rate insensitive, and for the circular plates considered here, including nominal strain-rate coefficients in the numerical simulations resulted in smaller displacements than seen in the experimental results. Hence, strain-rate sensitivity was not included in further numerical simulations here. It is important to note that for other materials, such as mild steel, the strain-rate sensitivity should be included (Liu and Jones 1987).

Tensile test simulation

As was mentioned in Section 4.4, since for the experimental impact tests considered here only plastic deformation was observed, failure was not required to define the material of the specimen plates. However, the experimental tensile tests used to obtain the material

mechanical properties were modelled using LS-DYNA both in order to verify that the impact model gave the correct plastic deformation, and also to make an initial attempt at failure prediction. For a purely plastic response without necking or fracture, the plastic parameters of the material can be determined from the results of a tensile test. However, fracture and necking occur over a length which is much smaller than the side length of the elements considered here and so the elements used in the finite element model cannot capture such a local phenomenon, and so to model failure, LS-DYNA deletes elements when their average strain reaches a 'critical' value.

This 'critial' value must be calibrated against test data (since the F.E. models can not simulate the experimental failure event at a small enough scale) and is a function of the element size (Simonsen and Lauridsen 2000). The mesh sensitivity can be approached with an engineering method at the level of advanced industry practice (Simonsen and Lauridsen 2000) in which the 'critical' failure strain (in this case the average normal strain over the element) required to give the actual experimental material fracture strain is found through numerical simulations of the tensile tests using different failure strains and mesh densities. Here 'failure strain' denotes the strain value when fracture occurs.

In the numerical simulations, only the length of the tensile test specimens between the clamping edges was modelled (Figure 7) and the same mesh sizes used in the circular specimen plates (Shell elements) were considered. The translational degrees of freedom were restricted at one end and at the other end a constant displacement of 100 times the experimental speed was prescribed (Ehlers 2009). Default hourglass control was included. The true stress-strain curve used to define the material was the same as that used for the circular plate specimens (Figures 5 and 6).

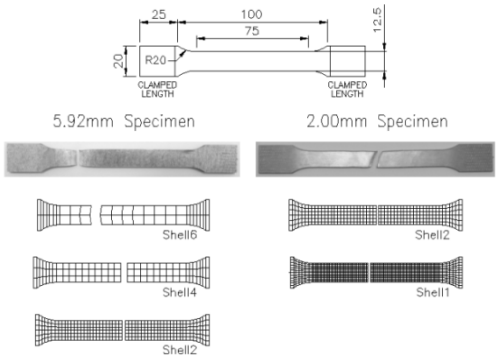

Figure 7: Tensile test specimens and their numerical simulation.

The material model for the tensile tests does not use a specific failure criteria in the purest sense, but the numerical simulation was 'calibrated' using the experimental data to give the 'critical' strain value (averaged over the element) that fitted the experimental results using a trial and error approach. For the tests carried out here, it was not difficult to estimate the first value of failure strain to be used since very little necking was observed in the experiments and thus the failure strain was close to the axial strain at the initiation of necking initiation. The force of the displaced nodes at the free end is obtained and this force plotted versus the applied prescribed displacement, and these values used to give the engineering stress-strain behaviour.

The results for different mesh sizes are presented in Figures 8 and 9 for thick and thin plates respectively. The 'critical' failure strain (used as input in the numerical model) represented in both graphs is 0.15. The dependences of the failure strain on the element size is evident from Figures 8 and 9 (a coarse mesh requires a minimum value of failure strain), showing that this parameter is not a true material property in this case. Most numerical simulations of tensile tests in the literature follow the engineering curve quite precisely until the point of necking independently of mesh size (even with relatively coarse meshes), but the post-necking behaviour is usually highly dependant on the mesh size (Simonsen and Lauridsen 2000, Tabri et al. 2007). For the aluminum 5083/H111 tensile tests carried out here, the stress at maximum load was almost coincident with the fracture stress and very little necking was observed (Figures 5 and 6). Hence, such post-necking modelling problems were avoided, and the plastic response could be equally well modelled using different mesh sizes.

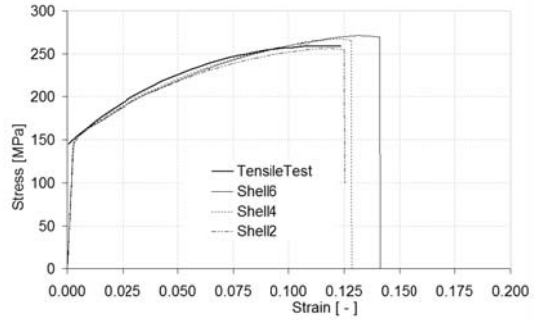

Figure 8: Numerical and experimental engineering stress-strain curves. Thickness 5.92 mm.

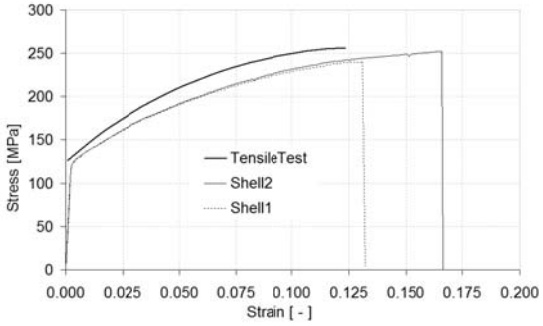

Figure 9: Numerical and experimental engineering stress-strain curves. Thickness 2.00 mm.

For the thick tensile test simulation, Figure 8 shows that all mesh sizes considered predicted well the plastic behaviour of the material. The fact that the Shell4 and Shell6 models overestimate the specimen failure strain show that a minimum value of the material failure strain would be required to be found for the coarser mesh sizes.

For the thin specimens the numerical simulation (Figure 9) for both mesh sizes considered give almost identical results, both giving approximately 8.0 % lower stress

values than the experimental results. Again it is indicated that for the coarser mesh Shell2 model, a minimum value for the material failure strain should be obtained to give a more approximated response compared with the experimental results. It is worth noting that the numerical simulations all predicted a fracture perpendicular to the specimen axis whereas in the thin tests this fracture was inclined (Figure 7). This is due to the fact that the fracture process occurs at a molecular scale well below that of the mesh size, and may be due to adjacent layers of atoms sliding over each other, resulting in a shear failure.

Numerical results and comparison with experimental tests

Firstly various numerical models using the different mesh sizes and element type referred to in Section 4 were evaluated in terms of ability to predict the experimental results. In order to do this a 'high' and a 'low' velocity impact (Table 1, shaded rows) was modelled for each plate thickness. Figures 10 to 13 compare the experimental force-displacement curves with those from the finite element calculation. Then this information will be used to select the 'best' models to proceed to calculate the maximum force and displacement values for the whole range of experimental impact velocities considered here.

For the thick plates Figures 10 and 11 show that, for both velocities, the Shell2 model approximates well the experimental plastic response, and that the coarser meshed Shell4 and Shell6 are less accurate. For the solid element models very similar results were obtained using both mesh sizes, but in terms of force-displacement prediction they do not give better predictions than the computationally less demanding Shell2 model.

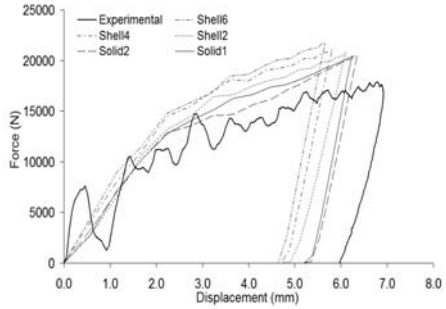

Figure 10: Force-displacement curves. Thick (5.92 mm) circular plates, impact velocity 5.85 m/s.

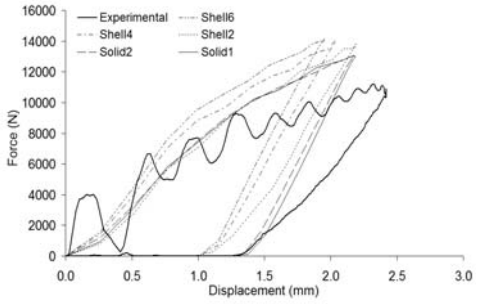

Figure 11: Force-displacement curves. Thick (5.92 mm) circular plates, impact velocity 2.62 m/s.

Again, for both impact velocities, the deflection at which this maximum force is reached is generally underestimated by the numerical models, consequently the maximum force is overestimated. Of the shell models, the Shell2 mesh gives the best prediction of this point, with both solid element models giving slightly better and very similar behaviour in this respect.

However, prediction of the impact response is not the only criterion; it is also beneficial to predict well the shape of deformation due to both local indentation and global deflection. Here it is relevant to remember that local 'indentation' can be thought of consisting of (i) local out of plane plate deformations (where the plate 'wraps around' the indenter) and also (ii) the actual indentation of the indenter into the thickness of the plate material.

Figure 14(a) shows that in this respect the Solid1 mesh gives a better definition of the shape of the deformation than does the Shell2 model. This is both because the finer mesh of the former is able to model more accurately the deformation around the indenter (c.f. (i) above), and because a solid element is able to model the change in thickness of the material due to the indentation (c.f. (ii) above).

Now considering the thin plates, Figures 12 and 13 show that all of the shell mesh sizes considered give a good representation of the plastic force-displacement behaviour, especially at the higher impact velocity, and that there is little to choose between them. The use of more computationally expensive solid elements gives a very good fit to the experimental data even at the low impact velocity, where the shell models over-estimate the force slightly.

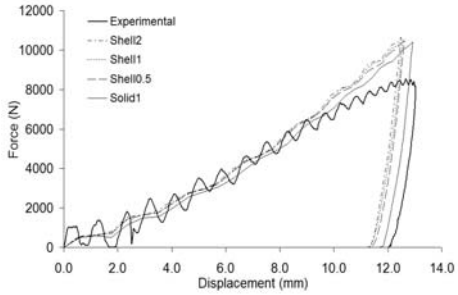

Figure 12: Force-displacement curves. Thin (2.00 mm) circular plates, impact velocity 5.90 m/s.

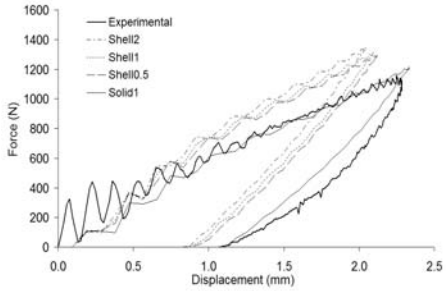

Figure 13: Force-displacement curves. Thin (2.00 mm) circular plates, impact velocity 0.95 m/s.

For the thin plates indentation is more significant in terms of out of plane plate deformation, but less significant in terms of indentation into the material thickness (Figure 14(b)). Hence, here the only requirement is a fine mesh to adequately model the

local deformation, with shell or solid elements giving similar representations.

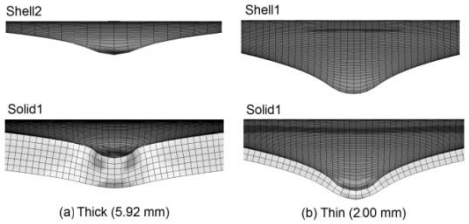

Figure 14: Shape of the deformation. (a) Thick (5.92 mm) circular plates, impact velocity 5.85 m/s. (b) Thin (2.0 mm) circular plates, impact velocity 5.90 m/s.

It should be noted at this point that though the experimental force-displacement curve is well but not always perfectly predicted by the numerical model, the time dependant curves of displacement and absorbed energy fit the experimental data very well.

The next step was to use the 'best' shell and solid models to simulate the remaining experimental impact velocities considered. As can be seen from figures 15 to 18 the models predict very well the maximum deflection and maximum force. It is also apparent that, *when considering maximum force and deflection values only*, there is little if any significant differences between the various models and hence little advantage in using a more computational expensive element model.

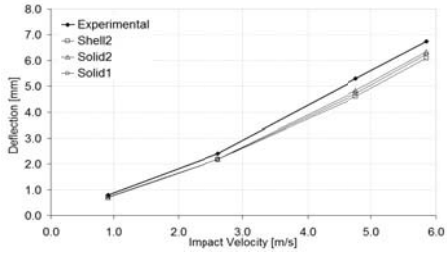

Figure 15: Maximum deflection vs. impact velocity. Thick (5.92 mm) circular plates.

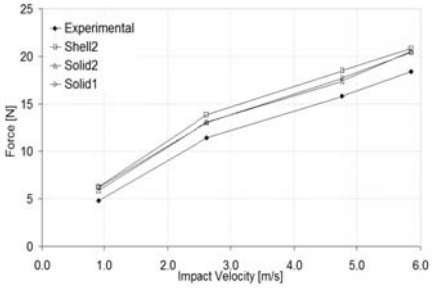

Figure 16: Maximum force vs. impact velocity. Thick (5.92 mm) circular plates.

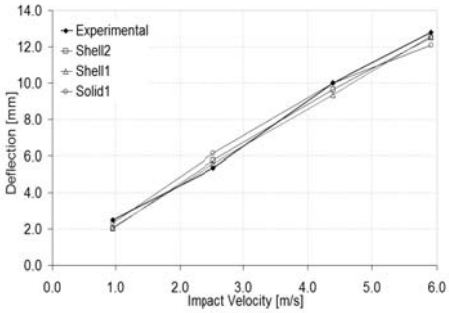

Figure 17: Maximum deflection vs. impact velocity. Thin (2.00 mm) circular plates.

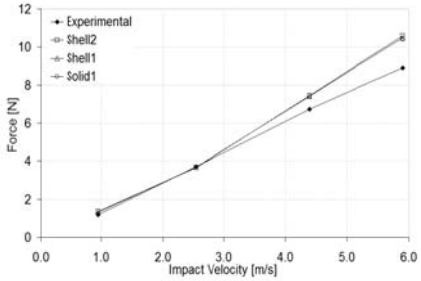

Figure 18: Maximum force vs. impact velocity. Thin (2.00 mm) circular plates.

The models showed that the maximum effective stress occurred on the lower surface opposite the impact point on both models shell and solid. The time variation of the effective stress is shown in Figure 19 for the thick circular plate with an incident velocity of 5.85m/s as an example. Stress is shown for elements on the upper and lower surface at both the impact point and at a point near the support. It can be seen from this figure that the maximum stress occurs on the surface opposite to the impact point, but that near the support the stresses are almost the same on both sides of the plate. The maximum effective stress distribution in the solid model is also plotted in Figure 20 for the same impact event.

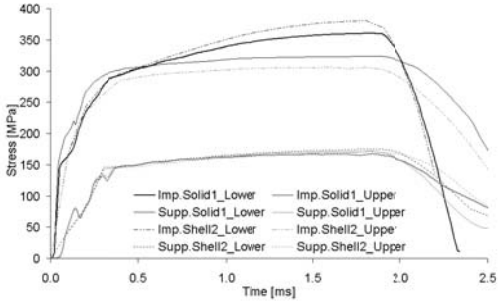

Figure 19: Effective stress with time. Thick (5.92 mm) circular plates, impact velocity 5.85 m/s.

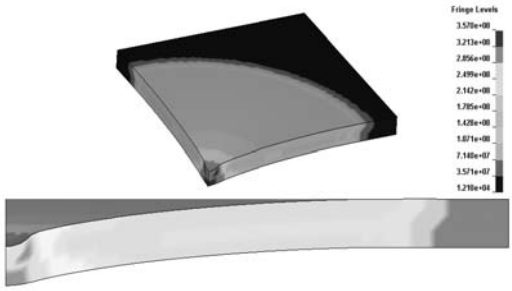

Figure 20: Maximum effective stress distribution. Thick (5.92 mm) circular plates, impact velocity 5.85 m/s.

The mass kinetic energy is dissipated as a combination of internal and sliding energies. For example, these values are plotted for the thick plate impacted at 2.62 m/s in Figure 21, where the magnitude of the sliding energy is about 13% of the dissipated kinetic energy using the Shell2 model, but only approximately 5% when either of the solid models are used. This implies that there is a small relative motion between the surface of the shell elements and the impacting mass, which is becoming less significant when solid elements are used. This could be because the

indentation into the material thickness is modelled only in the case of solid elements, hence resisting sliding, but this is not clear and requires further investigation.

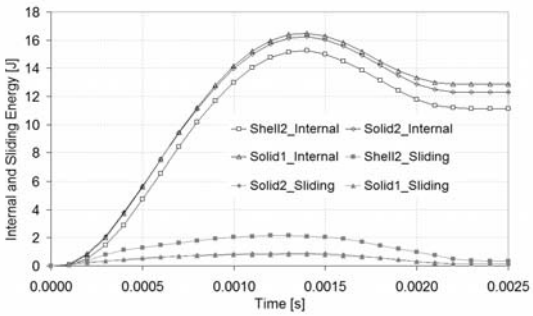

Figure 21: Internal and sliding energy dissipation. Thick (5.92 mm) circular plates, impact velocity 2.61 m/s.

Overall, good agreement between numerical and experimental results was obtained, especially for the thin plates. However, for the thick plates some discrepancies between theory and test results differences were noted, the possible reasons for which are discussed below:

It is possible that the actual experimental clamped condition was not as perfect as represented in the numerical model; it is quite possible that some slippage between the support plates was experienced by the specimen plate, and in fact all of the tested plates experienced greater displacements than predicted by the finite element models. The numerical clamped condition is affected by the static coefficient of friction in the contact definition between support and specimen plates, for example decreasing this coefficient gives greater displacements and lower forces, giving a better approximation between experimental and numerical results. Further work would be beneficial to further refine the model in terms of this coefficient.

The true stress-strain curve material definition input to the numerical model is also a possible source for discrepancies; here these values were obtained using tensile tests specimens cut from the same plates from which the impact specimens were taken, & the data differed from that supplied by the plate manufactures. Another possible material property source of errors is the strain-rate effect, which was not considered in the current numerical model. A search of the literature showed that Cowper-Symonds data for aluminium 5083/H111 is not available, and since these coefficients have been seen to vary greatly between specific aluminium alloys, values for other alloys could not be used. Preliminary studies into the effect of strain rate have showed that further work to obtain this data could improve the accuracy of the maximum displacement results calculated here.

A further possible source of differences between the finite element and experimental results is the oscillations seen during the impact response (experimental force-time curves), which were not separated from the mechanical loads. This effect could be due to vibrations in the striking mass assembly or material vibrations around the indentation stiffness, and the development of a more complex geometrical model would help to clarify the source of these effects.

Generally, in this study some of the parameters that affect the impact response were varied to optimise the finite element model (e.g. mesh size and element type), but others were set at constant values obtained from the literature or not included (e.g. static coefficient of friction and strain-rate parameters) in order to keep the size of the investigation practicable. However, further work could now investigate the effects of all of the parameters, especially if labour-saving techniques such as those of statistical experimental design (Sutherland and Guedes Soares 2003) were used to ensure a practical number of modelling runs and, importantly, to ensure that any interactions between these parameters are correctly identified.

Conclusions

Detailed information of the impact response of clamped aluminium 5083 circular plates has been obtained through non-linear explicit dynamic simulation using the LS-DYNA software package. The results obtained were in good agreement with those of previous experimental tests, indicating that even computationally inexpensive coarse meshes using shell elements are sufficient to predict the maximum deflections and forces. However, finer meshed shell and solid element models give better and best prediction of the force-displacement behaviour, respectively. Where small discrepancies between numerical and experimental results occurred, this was due to overestimation of the impact force; the variation of displacement with time is generally very well predicted.

The numerical simulations give a good understanding of the shape of the deformation in plates subjected to impact loading, and a fine meshed solid model is needed to give a good approximation of the deformation shape, especially where local indentation is significant. In the present work the study of the effect of mesh size showed that the ratio of element size to indenter radius should preferably be approximately 1/5 in order to satisfactorily define the shape of the deformation.

The material true stress-strain curve inputs to the numerical model were obtained from tensile tests on the actual material used to fabricate the impacted plates. This was simplified since the test maximum load was almost coincident with the rupture load, but for other materials is may be more difficult to define the true stress-strain curve and some approximations as the power law curve must be included.

The numerical models were successfully used to predict the impact response of Aluminium 5083 plates, and the next planned stage of this work is to see if the technique is also successful for steel plate impact tests. For example, strain-rate does not seem to play an important role in numerical simulation of these aluminium plates, however this may not be the case for other materials.

Acknowledgments

The work has been performed in the scope of the project MARSTRUCT, Network of Excellence on Marine Structures (http://www.mar.ist.utl.pt/marstruct/), which has been financed by the EU through the GROWTH Programme under contract TNE3-CT-2003-506141.

The first author has been financed by the Portuguese Foundation for Science and Technology (Fundação para a Ciência e Tecnologia), under contract SFRH/BD/46369/2008.

References

Akita Y, Ando N, Fujita Y, Kitamura K. 1972. Studies on collision-protective structures in nuclear powered ships. Nucl Engng Des. 19: 365 - 401.

Amdhal J, Kavlie D, Johansen A. 1995. Tanker grounding resistance. Proc. 6th Int. Symp. on Practical Design of Ships and Mobile Units (PRADS'95). 1072 - 1083.

Dieter GE. 1986. Mechanical behavior under tensile and compressive loads. ASM Handbook. 8: 99-10.

Ehlers S. 2010. Strain and stress relation relation until fracture for finite element simulations of a thin circular plate. Thin-Walled Structures. 48 (1): 1 - 8.

Ehlers S, Varsta P. 2009. Strain and stress relation for non-linear finite element simulations. Thin-Walled Structures. 47 (11): 1203 - 1217.

Ehlers S, Klanac A, Tabri K. 2007. Increased safety of a tanker and ropax vessel by implementing a novel sandwich structure. 4th International Conference on Collision and Grounding of Ships: Hamburg, Germany. 109 - 115.

Guedes Soares C. 1981. A Mode solution for the finite deflections of a circular plate loaded impulsively. Engineering Transactions. 29 (1): 99 - 114.

Hallquist JO. 2005. LS-DYNA Theory Manual. Livermore Software Technology Corporation.

Jones N. 1989. Structural Impact. Cambridge University Press.

Kajaste-Rudnitski J, Vastra P, Matusiak J. 2005. Some finite element estimates of ship collision event. Maritime Transportation and Exploitation of Ocean and Coastal Resources, Taylor & Francis Group, London. 447 – 453

Liu J, Jones N. 1987. Experimental investigation of clamped beams struck transversely by a mass. International Journal of Impact Engineering. 6 (4): 305 - 335.

McDermott JF et al. 1974. Tanker structural analysis for minor collision. Trans SNAME. 82: 382 - 407.

Shen WQ. 1995. Dynamic plastic response of thin circular plates struck transversely by nonblunt masses. Int. J. Solids Structures. 32 (14): 2009 - 2021.

Shen W.Q. 2002. A study on the failure of circular plates struck by masses. Part 2: theoretical analysis for the onset of failure. International Journal of Impact Engineering 27 (4): 413 - 432.

Shen WQ, Rieve NO, Baharun B. 2002. A study on the failure of circular plates struck by masses. Part 1: experimental results. International Journal of Impact Engineering. 27 (4): 399 - 412.

Simonsen BC, Lauridsen LP. 2000. Energy absorption and ductile failure in metal sheets under lateral indentation by a sphere. International Journal of Impact Engineering. 24 (10): 1017 - 1039.

Stronge WJ, Yu TX. 1993. Dynamic Models for Structural Plasticity. © Springer-Verlag London Limited.

Sutherland LS, Guedes Soares C. 2003. The effects of test parameters on the impact response of glass reinforced plastic using an experimental design approach. Composites Science and Technology. 63: 1 - 18.

Sutherland LS, Guedes Soares C. 2009. Impact behaviour of GRP, aluminium and steel plates. Analysis and Design of Marine Structures; Guedes Soares & Das (eds). Taylor & Francis Group: London. 293 – 300

Tabri K, Alsos H, Broekhuijsen J, Ehlers S. 2007. A benchmark study on ductile failure criteria for shell elements in multiaxial stress state. Advancements in Marine Structures, Guedes Soares & Das (eds). Taylor & Francis Group: London. 401-409.

Wang G, Ohtsubo H, Arita K. 1998. Large deflection of a rigid-plastic circular plate pressed by a sphere. Journal of Applied Mechanics. 65 (2): 533 - 535.

Wang G, Ohtsubo H, Liu D. 1997. A simple method for predicting the grounding strength of ships. J Ship Res. 41: 241 - 247.

Yu TX, Chen FL. 2000. Failure of plastic structures under intensive dynamic loading: Modes, criteria and thresholds. Int. J. of Mechanical Science. 42: 1531 - 1554